Academia Journal of Scientific Research 5(8): 000-000, August 2017
DOI: 10.15413/ajsr.2017.0629
ISSN 2315-7712

Academia Publishing

CrossMark click for updates

Research Paper

Enhancing the performance of quasi-solid state dye-sensitized solar cells by using rGO-TiO_2 composite photoelectrodes

Thiago F. P. da Silva[1]*, Paulo Alliprandini[1], Helder J. Ceragioli[2], Alfredo C. Peterlevitz[2], João E. Benedetti[3] and Agnaldo D. Gonçalves[3]

[1]Institute of Engineering, Sciences and Technology, Federal University of Jequitinhonha and Mucuri Valleys, UFVJM, P.O. Box 39.440-000, Janaúba, MG, Brazil.
[2]Department of Semiconductors, Instruments and Photonics, School of Electrical and Computer Engineering, University of Campinas – UNICAMP, P.O. Box 6101 13083-970, Campinas, SP, Brazil.
[3]Institute of Sciences and Technology, Paulista University, UNIP, P.O. Box 13485-342, Limeira, SP, Brazil.

*Corresponding author. E-mail: thiago.franchi@ufvjm.edu.br. Tel: +55 38 3829 3100; Fax: +55 38 3829 3100.

Accepted 10th August, 2017

ABSTRACT

The incorporation of carbon compounds was exploited to improve the efficiency of solar cell, although, most of the incorporation utilize the chemical route. In this study, we proposed an alternative route utilizing a vapour deposition. The reduced graphene oxide (rGO) was prepared by hot filament chemical vapor deposition (HFCVD). The formation of graphene oxide is evidenced by Raman spectra from the characteristic signals at 1345 and at 1594 cm^{-1}, respectively. Scanning electron microscopy (SEM) images from rGO samples showed a rough surface with high surface area. Results from thermogravimetric analyses (TGA) indicated a decomposition temperature of ca. 450°C for rGO samples synthesized by HFCVD, which is suitable for the heat treatment conditions usually employed when processing photoelectrodes for dye-sensitized solar cells (DSCs). Quasi-solid state DSCs were assembled from composite photoelectrodes based on TiO_2 and rGO. Composite photoelectrodes were prepared by using TiO_2 nanoparticles and rGO samples in different ratios in the paste composition. Quasi-solid state DSCs based on composite photoelectrodes and a gel polymer were assembled with Pt counter electrodes. It was possible to prepare uniform, crack-free TiO_2 layers by using large quantities of rGO and the energy conversion efficiencies improved by increasing rGO loading in the photoelectrode.

Keywords: Hot filament chemical vapor deposition (HFCVD), reduced graphene oxide (rGO), carbon compounds, solar cell.

INTRODUCTION

Even though the sun is an unlimited source of energy, solar energy conversion has not been fully explored. For that purpose, devices must become more efficient in harvesting and then converting sunlight into electricity. Under this scenario, dye-sensitized solar cells (DSCs) greatly improved by O' Regan and Grätzel (1991) attracted significant attention as a promising solution *in lieu* of costly solar cell technologies based on inorganic semi-conductors (Burschka et al., 2013).

The traditional architecture of DSCs entails a stack of layers from different components: a porous nanostructured TiO_2 layer as photoelectrode (PE) and usually a platinum thin film as the catalytic layer for the counter-electrode (CE), both deposited on the surface of a transparent conducting substrate, for example, a glass substrate coated with a thin film of fluoride-doped tin oxide (FTO) (Avellaneda et al., 2010; White et al., 2011). Since TiO_2 has a weak absorption in the visible range, light-absorbing species are usually attached to its surface, acting as sensitizers.

A liquid electrolyte containing a redox couple, usually I^-/I_3^-, is inserted in between the electrodes (PE and CE). The working principle of this device is very simple; sunlight is absorbed by the photoelectrode, which is composed of a dye-sensitized porous nanostructured TiO_2 layer deposited onto a transparent conductor oxide substrate. Electrons are then injected into the conduction band of the semi-conductor oxide from the excited state of the dye. This process is very efficient (yield of ca. 100%) and ultrafast (fs) for some dyes (Haque et al., 2005; Matar et al., 2008). These electrons are transported through the electrical

circuit, generating electricity and then they reach the counter-electrode (a thin film of Pt onto a transparent conductor oxide substrate), wherein triiodide ions (I_3^-) are present in the liquid electrolyte composition (usually I_2 and LiI in acetonitrile). Since the system is regenerative, the dye is re-reduced by the iodide (I) anions, which is a redox pair in conjuction with I_3^- in the electrolyte. This process is also very efficient, approximately, 100 ns, depending on the voltage applied (Kong et al., 2007).

The best efficiency values achieved so far by DSCs have been maintained within a stable plateau of ~ 13% (Mathew et al., 2014; Sauvage et al., 2010). These values are lower than those reported by devices based on inorganic materials, such as silicon, which have shown efficiencies larger than 25% (Green et al., 2014).

One of the drawbacks associated with the poor efficiencies of DSCs are the recombination processes taking place in the device (Barnes et al., 2009). The recombination processes in the semi-conductor interface are one of the main reasons behind the poor conversion efficiency in DSCs (Barnes et al., 2009).

The photoinjected electron from the excited state of the dye into the conduction band of TiO_2 might recombine with the electrolyte or re-reduce the dye cation (Green et al., 2014). It is usually accepted that the electrons injected into the semi-conductor oxide by the excited state of the dye are transported by a diffusion process. Electron diffusion in the semi-conductor oxide is not very efficient due to surface defects, which allow recombination processes from photogenerated charges and these processes contribute to decrease device performance (Rensmo et al., 1997). The chemical diffusion coefficient for electrons in the nanostructured porous film is ca. 10^{-5} cm^2 s^{-1} (Enright and Fitzmaurice, 1996) which is smaller than the value calculated for bulk materials (ca. 10^{-2} cm^2 s^{-1}) (O'Regan et al., 1990).

An interesting approach to decrease recombination processes consists in improving electron transport in the nanostructured TiO_2 porous layer, which may be done by means of incorporating conducting materials into the ink composition, such as carbonaceous materials (Xia et al., 2007). Studies from Morais et al. (2012) showed that TiO_2 photoelectrodes containing multiwall carbon nanotubes (MWCNT) dispersed among semi-conductor oxide nanoparticles provide more efficient electron transport increasing the efficiency of solar cells (O'Regan et al., 1990).

As well as carbon nanotubes, graphene is a promising candidate for this purpose due to its excellent conductivity (Park et al., 2011) resistance against photodegradation and high surface area (Balandin et al., 2008; Geim and Novoselov, 2007). Therefore, the HFCVD technique was employed herein for synthesizing high quality graphene samples for application as composite photoelectrodes for improving DSC performance. The CVD technique consists of a decomposition of a vapor or gas precursor composed of carbon atoms, usually a hydrocarbon, in the presence of a metal catalyst under inert atmosphere at a temperature generally lower than 1000°C (Chen and Wang, 2010).

The nucleation and growth of graphene oxide takes place due to the presence of carbon atoms arising from the precursor decomposition. The aim of this work is to employ rGO samples synthesized by HFCVD for preparing composite photoelectrodes to be applied in quasi-solid state DSCs. rGO is expected to improve electron transport from TiO_2 nanoparticles to charge collectors (Kavan et al., 2011), thus, significantly improving the performance of DSCs.

MATERIALS AND METHODS

Preparation of reduced graphene oxide by HFCVD

Reduced graphene oxide (rGO) was prepared from a catalytic conversion by using a copper substrate. A solution of polyaniline (PANI) in 1 ml of dimethylformamide (DMF) was dropped onto the copper substrate and then dried at room temperature for 2 h. Afterwards, a nickel nitrate solution (0.2 mol L^{-1}) in acetone was dropped over the PANI-covered substrate. The copper substrate was then put inside a hot filament chemical vapor deposition reactor.

The reactor is fed by a carbon source composed of a mixture of camphor, acetone and citric acid, which is under hydrogen bubbling (15%). The resulting vapor is then carried into the reactor. The pressure inside the reactor was 20 Torr, wherein there is a tungsten (W) wire at a temperature of 2000°C. The overall gas flow is at 100%, which is constantly monitored. Substrate temperature was kept at 450°C and monitored by a thermocouple on top of the substrate.

Polymer electrolyte preparation

The polymer electrolyte was prepared by following the procedure described by Benedetti et al. (2010). The electrolyte was prepared by dissolving 0.3 g of the P(EO/EM) copolymer and 0.7 g of gamma-butyrolactone (GBL) in 5 ml of acetone. The copolymer, additive (GBL) and solvent were kept under stirring for 72 h inside a sealed vessel. Afterwards, 0.2 g of LiI and 0.02 g of I_2 were added. The solution was left sealed and under stirring for 72 h before use.

Photoelectrode

Five TiO_2 paste compositions were prepared by adding TiO_2 nanoparticles (P25 Evonik) and different rGO amounts: sample A with 0.5 mg, sample B with 1.0 mg, sample C with 1.5 mg, sample D with 2.0 mg and sample E with 3.0 mg. The paste was prepared by adding 3.0 g of TiO_2 (P25, Evonik), 1.2 g of PEG 20000, 5 ml of distilled water, 0.1 ml of acetylacetone and Rgo in the quantities earlier mentioned (samples A, B, C, D and E, respectively).

A small amount of the TiO_2 paste was dropped over the transparent conducting oxide substrate (fluoride-doped tin oxide, SnO_2: F – FTO, Hartford, USA) and then applied by the doctor blading technique. Scotch tape (3 M) was used as frame and spacer. The resulting layers were dried for 30 min and then submitted to a heat treatment of 350°C for 15 min, followed by 450°C for 30 min at a heating rate of 10ºC/min (EDG, model EDG3P–S).
Film thickness was measured by using a Taylor Hobson profilometer, model Form Talysurf Intra. Sensitization was carried out by using a 1 mmol L^{-1} of the N-719 dye (Solaronix, used without further purification) overnight. Counter-electrodes were deposited by sputtering thin Pt films (400 Å) onto FTO substrates.

Solar cell assembly

A small amount of the polymer electrolyte was dropped onto the N-719-sensitized photoelectrode (FTO/TiO_2/dye) heated over a hot plate at 50°C for 20 min for solvent evaporation. A Pt counter electrode was then pressed against the electrolyte-covered photoelectrode in a sandwich configuration. In order to avoid short-circuit scotch tape was used as spacer (50 µm).

Electrical measurements (*J-V* curves)

J-V curves were measured under AM1.5 illumination (100 mW cm^{-2}) by using an Orbital solar simulator, model AM15 × 100 (class C, from Orbital Engenharia, Brazil). An Autolab PGSTAT-30 potentiostat was used for data acquisition. *J-V* curves were measured also in the dark. The data were fitted by using the CurrentModel software.

Raman spectroscopy

The Raman spectra of the rGO samples and TiO_2 porous layers were measured in a Renishaw System 2000 Raman spectrometer under Ar laser excitation (λ = 514.5 nm and 633 nm) at a power of 6 mW.

Thermal measurements

Thermogravimetric analyses as a function of temperature were measured for rGO samples in a thermogravimetric analyser, model TGA 2950, from TA Instruments. The analyses were performed under an argon flow of 100 ml/min. Samples were heated from room temperature up to 500°C at a heating rate of 10°C/min.

Field emission gun scanning electron microscopy (FEG-SEM)

Morphological analyses were carried out by using a JEOL6330F scanning electron microscope at an operating voltage of 5 kV.

High-resolution transmission electron microscopy (HR-TEM)

HR-TEM measurements were performed in a JEOL3010 High-Resolution Transmission Electron Microscope.

RESULTS AND DISCUSSION

Raman spectroscopy

Raman spectroscopy is a versatile tool for studying graphene structural properties. The G line usually appears at ca. 1582 cm^{-1}, whereas the D line appears at ca. 1350 cm^{-1} (Wang et al., 2008). Bands at 1345, 1594, 2692, 2911 and 3248 cm^{-1} were observed in the Raman spectra of rGO samples prepared by HFCVD (Figure 1). The bands at 1345 cm^{-1} (higher intensity) and at 1594 cm^{-1} (lower intensity) in Figure 1A characterize the HFCVD samples as graphene oxide.

The harmonic contributions from the D and G lines, referred as D' and G', appear at 2700 and at 3248 cm^{-1}, respectively. In graphite, the G line is more intense than the D line, whereas the D' line is very weak and the G' is very intense. In the Raman spectrum of graphene oxide, the G line is shifted to 1595 cm^{-1} and the intensity of the D line at 1350 cm^{-1} increases significantly. This phenomenon may be assigned to the significant decrease in the sp^2 size domain due to oxidation and the partially ordered rGO sheet structure (Wang et al., 2008; Stankovich et al., 2007).

The Raman spectrum in Figure 1B has bands at 141, 397, 513 and 639 cm^{-1}, respectively. These signals characterize anatase, one of the three mineral phases of TiO_2 represented by 3 bands at 395, 518 and 642 cm^{-1} (Park et al., 2011). Anatase is the most stable phase of TiO_2 in the nanometer scale, which is also the most studied for nanotechnology applications (Parkin, 2005; Ibhadon, 2013).

The Raman spectrum of the rGO-containing TiO_2 photoelectrode in Figure 1C shows all the characteristic bands of TiO_2, along with the main signals associated to graphene oxide. This result suggests no degradation to the graphene crystalline structure, even after the heat treatment, which corroborates the presence of graphene embedded into the TiO_2 porous layer. Another evidence for the presence of rGO is the color of composite photoelectrodes. The higher the graphene loading, the darker the photoelectrode becomes even after heat treatment.

Field emission gun scanning electron microscopy (FEG-SEM)

Figure 2A shows SEM images of rGO samples synthesized

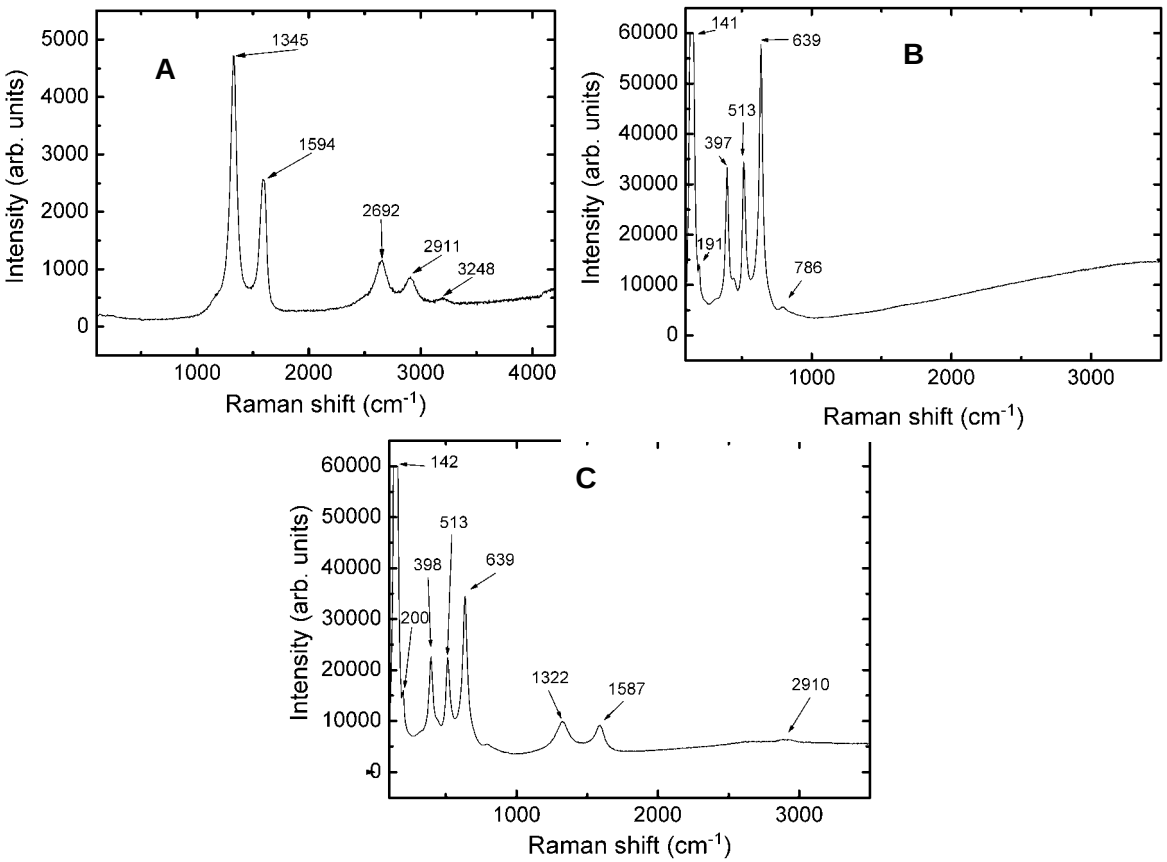

Figure 1: (A) Raman spectrum of the rGO sample synthesized by HFCVD; (B) Raman spectrum of the TiO_2 porous layer heat-treated at 450°C for 30 min; (C) Raman spectrum of the rGO-containing TiO_2 photoelectrode (2.0 g – sample D) heat-treated at 450°C for 30 min.

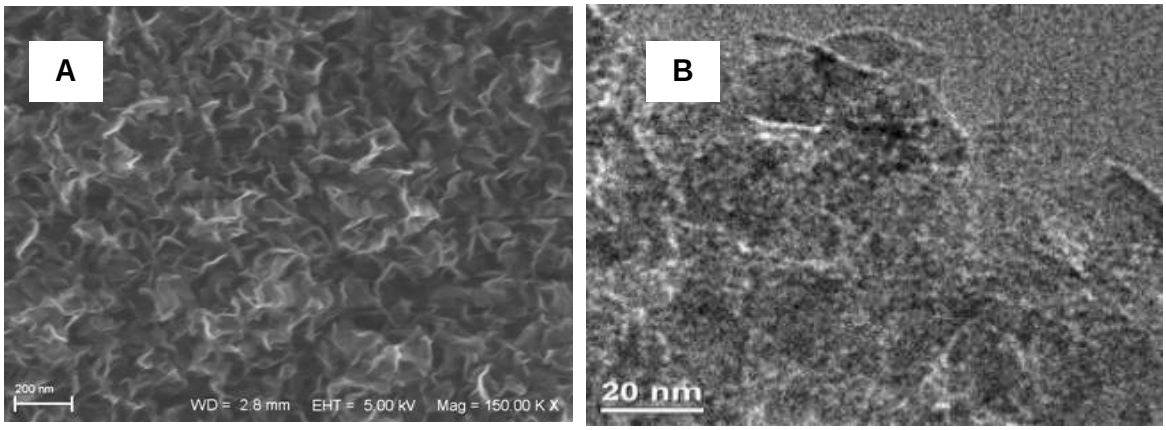

Figure 2: (A) FEG-SEM image of an rGO sample prepared by HFCVD; (B); HR-TEM image of an rGO sample prepared by HFCVD.

by HFCVD. The morphology of rGO samples synthesized by HFCVD resembles wrinkled paper sheets (Figure 2A) with a smooth surface (Ismail et al., 2013). This morphology is similar to that reported for graphene synthesized by the Hummers method (Park et al., 2011; Zhang et al., 2010). This morphological property allows high electrical conductivities and surface area to the material (Ismail et al., 2013). Therefore, even small loadings of carbonaceous materials allow considerable gains in electrical conductivity for TiO_2 layers. Subsequently, additional results for morphological characteristics of rGO samples synthesized by HFCVD are provided.

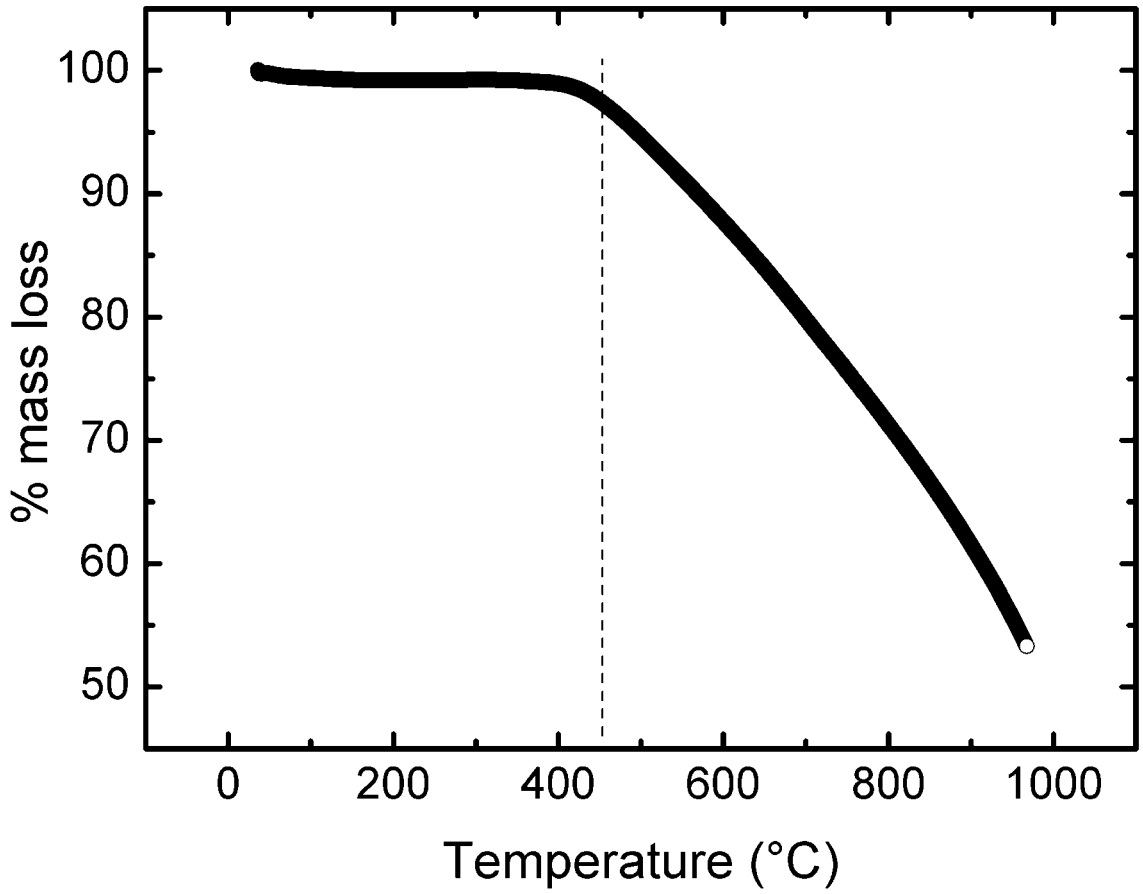

Figure 3: TGA curve for a sample of rGO prepared by HFCVD.

High-resolution transmission electron microscopy (HR-TEM)

HR-TEM images in Figure 2B shows the edges of the rGO sheets, which evidences thicknesses of a few nanometers (He et al., 2012). The thickness for the rGO sheets in this work suggests the presence of stacked plaques of a few hundred graphene sheets, which provides a relatively high surface area for the growth of TiO_2 nanoparticles during the sintering process. The effectiveness of sintering is important for neck growth, which is another path for electron diffusion up to the FTO substrate (Yuan et al., 2012).

Thermogravimetric analyses (TGA)

Figure 3 shows the TGA curve for the rGO powder sample. The decomposition temperature can be considered when there is 5% weight loss. For the rGO samples prepared by HFCVD in this work, it is possible to infer that the decomposition temperature is around 450°C. This result evidences the existence of a few oxygen-containing groups (Chen and Wang, 2010; Yuan et al., 2012).

Current-voltage curves (*J-V* curves)

Six photoelectrodes were prepared with different rGO loading in the TiO_2 paste: 0 (control), 0.5, 1.0, 1.5, 2.0 and 3.0 g, respectively. Quasi-solid state DSCs based on composite photoelectrode and a gel polymer electrolyte with excellent mechanical stability were assembled with Pt counter electrodes.

Figure 4 shows the *J-V* curves measured under illumination of 100 mW cm^{-2} for DSCs based on photoelectrodes composed of: A: 0.5 mg of rGO, B: 1.0 mg of rGO, C: 1.5 mg of rGO and D: 2.0 mg of rGO.

Energy conversion efficiencies improved by increasing rGO loading in the photoelectrode up to 2.0 g. Table 1 shows the short-circuit current (J_{SC}), open-circuit voltage (V_{OC}), fill factor (FF), energy conversion efficiency (η) and series resistance (R_s) for DSCs based on rGO-containing TiO_2 photoelectrode.

It was possible to observe that an increase in the graphene oxide concentration provided an improvement of ca. 83% on J_{sc}. However, V_{oc} dropped somewhat, as well as the FF. The composite photoelectrode with 2.0 g of rGO (sample D) provided DSCs with the lowest series resistance (R_s – Table 1), which evidences the electrical conducting

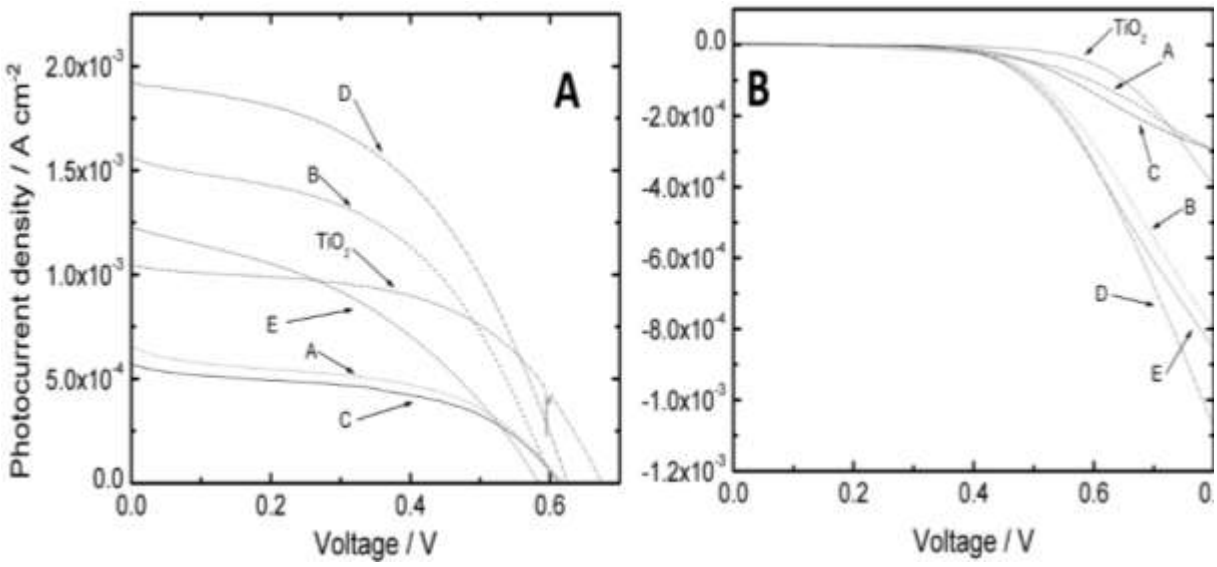

Figure 4: *J-V* curves of DSCs based on rGO-containing TiO_2 photoelectrodes: (A) under 100 mW cm^{-2} illumination (AM1.5) and (B) in the dark. A stands for 0.5 mg of rGO, B for 1.0 mg of rGO, C for 1.5 mg of rGO, D for 2.0 mg of rGO and E for 3.0 mg of rGO.

Table 1: Electrical parameters from the *J-V* curves (AM 1.5, 100 mW cm^{-2}) measured from DSCs based on TiO_2 and rGO-containing TiO_2 photoelectrodes. Active solar cell area: 0.25 cm^2.

rGO loading (g)	J_{sc} (mA cm^{-2})	V_{oc} (V)	*FF*	η (%)	R_s (Ω cm^{-2})
0	4.2	0.68	0.54	1.5	165
0.5	2.3	0.61	0.50	0.7	240
1.0	6.3	0.60	0.48	1.8	142
1.5	2.6	0.62	0.47	0.8	274
2.0	7.7	0.63	0.48	2.3	100
3.0	4.93	0.58	0.40	1.2	175

properties of rGO to the TiO_2 nanostructured porous layer. The performance dropped with higher rGO loadings probably due to filtering effects, since the higher graphene content would block light transmission through the photoelectrode.

Conclusions

It was possible to prepare uniform, crack-free TiO_2 layers, even by using large quantities of rGO. The adhesion of the rGO-containing TiO_2 porous layers provided suitable mechanical properties for assembling DSCs. The growth of rGO samples by HFCVD was studied by FEG-SEM, HR-TEM, Raman spectroscopy and thermogravimetric analyses (TGA). TGA evidenced that rGO has poorer thermal stability than graphite, which is probably due to structure sizes. The degradation of this material begins only at temperatures higher than 450°C, confirming that even after the heat treatment of the rGO-containing TiO_2 photoelectrodes, graphene properties are preserved.

This result evidences that there is no by-product with another crystal structure. This is also observed in the Raman spectra, which clearly show characteristic bands of the graphene structure. The increase in the rGO concentration provided a higher J_{sc}, but V_{oc} dropped. However, the power extracted from the device increases by the addition of rGO into the TiO_2 paste. The alternative route using HFCVD will enable reduce the fabrications costs of the photovoltaic cells through the substitution of platinum counter-electrodes by reduced graphene oxide (rGO) and the elimination of PFO in the windows of photovoltaic using the reduced graphene oxide. This alternative rote can be used in many applications, like counter-electrodes for super capacitors etc.

ACKNOWLEDGMENTS

The authors wish to appreciate FAPESP (2012/08039-0 ADG) for the financial support; LME/LNLS for providing technical support for electron microscopies and LMF/LNLS

for preparing platinized counter-electrodes.

REFERENCES

Avellaneda CO, Gonçalves AS, Benedetti JE, Nogueira AF(2010). Electrochim. Acta 55:1468-1474.

Balandin AA, Ghosh S, Bao WZ, Calizo I, Teweldebrhan D, Miao F, Lau CN (2008). Nano Letters. 8:902-907.

Barnes PRF, Anderson AY, Koops SE, Durrant JA, O'Regan BC (2009). J. Phys. Chem. C. 113:1126-1136.

Barnes PRF, Liu L, Li X, Anderson AY, Kisserwan H, Ghaddar TH, Durrant JR, O'Regan B (2009). Nano Lett. 9:3532-3538.

Benedetti JE, Gonçalves AS, Formiga ALB, Paoli MA, Durrant JR, Nogueira AF (2010). J. Power Sources. 195:1246-1255.

Burschka J, Pellet N, Moon SJ, Baker RH, Gao P, Mohammad MK, Nazeeruddin K, Gratzel M (2013).Nature. 499:316-320.

Chen SQ, Wang Y (2010). J. Mater. Chem. 20:9735–9739.

Enright B, Fitzmaurice D (1996). J. Phy. Chem. 100:1027–1035.

Geim AK, Novoselov KS (2007). Nature Materials. 6:183-191.

Green MA, Emery K, Hishikawa Y, Warta W (2014). Prog. Photovoltaics Res. Appl. 22:701-710.

Haque SA, Palomares E, Cho BM, Green ANM, Hirata N, Klug DR, Durrant JR (2005). J. Am. Chem. Soc. 127:3456-3462.

He GY, Huang J, Liu WF, Wang X, Chen HQ, Sun XQ (2012). Materials Technol. 27:278- 283.

Ibhadon AO, Fitzpatrick P (2013). Catalysts. 3:189-218.

Ismail AA, Geioushy RA, Bouzid H, Al-Sayari SA, Al-Hajry A, Bahnemann DW (2013). Applied Catalysis B: Environ. 129:62–70.

Ismail AA, Geioushy RA, Bouzid H, Sayari SAA, Al-Hajry A, Bahnemann DW (2013). Applied Catalysis B: Environ. 129:62– 70.

Kavan L, Yum JH, Nazeeruddin MK, Gratzel M (2011). ACS Nano. 5:9171–9178.

Kong FT, Dai SY, Wang KJ (2007). Advances in OptoElectronics.1-13.

Matar F, Ghaddar TH, Walley K, Dos Santos T, Durrant JR, O'Regan B (2008). J. Mater. Chem. 18:4246-4253.

Mathew S, Yella A, Gao P, Humphry-Baker R, Curchod BFE, Ashari-Astani N, Tavernelli I, Rothlisberger U, Nazeeruddin MK, Grätzel M (2014). Nature Chemistry. 6:242-247.

Morais A, Loiola IML, Benedetti JE, Gonçalves AS, Avelhaneda CAO, Nogueira AF, J Clerici JH, Cotta MA (2012). Sol. Energ. Mat. Sol. Cells. 112:1-42.

O' Regan B, Grätzel M (1991). Nature. 353:737–740.

O'Regan B, Moser J, Anderson M, Gratzel M (1990). J. Phy. Chem. 94:8720–8726.

Park S, An J, Potts JR, Velamakanni A, Murali S, Ruoff RS (2011). Carbon. 49:3019-3023.

Park S, An J, Potts JR, Velamakanni A, Murali S, Ruoff RS (2011). Carbon. 49:3019-3023.

Parkin VI, Palgrave RG (2005). Materials Chem. 15:1689-1695.

Rensmo H, Keis K, Lindström H, Södergren S, Solbrand A, Hagfeldt A, Lindquist SE, Wang LN, Muhammed M (1997). J. Phys. Chem. B. 101:2598-2601.

Sauvage F, Chen D, Comte P, Huang F, Heiniger LP, Cheng YB, Caruso RA, Graetzel M (2010). Acs Nano. 4:4420-4425.

Stankovich S, Dikin DA, Piner RD, Kohlhaas KA, Kleinhammes A, Jia Y, Nguyen ST, Ruoff RS (2007). Carbon. 45:1558-1565.

Wang G, Yang J, Park X, Gou B, Wang H (2008). J. Phys. Chem. C. 112:8192-8195.

White RC, Benedetti JE, Gonçalves AS, Romão W, Vaz BG, Eberlin WN, Correia CRD, De Paoli MA, Nogueira AF (2011). J. Photochem. Photobiol. A. 222:185-191.

Xia XH, Jia ZJ , Yu Y , Liang Y, Wang Z, Ma LL (2007). Carbon. 45:717-721.

Yuan XY, Zou LL, Liao CC, Daí JW (2012). Express Polymer Letters 6:847–858.

Zhang YH, Tang ZR, Fu XZ, Xu YJ (2010). *Acs Nano*. 4:7303-7314.